ADVANCED FUNCTIONAL MATERIALS
www.afm-journal.de

Materials Views
www.MaterialsViews.com

# Diagrammatic Separation of Different Crystal Structures of $A_2BX_4$ Compounds Without Energy Minimization: A Pseudopotential Orbital Radii Approach

By *Xiuwen Zhang* and *Alex Zunger**

**The $A_2BX_4$ family of compounds manifest a wide range of physical properties, including transparent conductivity, ferromagnetism, and superconductivity. A 98% successful diagrammatic separation of the 44 different crystal structures of 688 oxide $A_2BX_4$ compounds (96% for 266 oxide-only) is described by plotting the total radius of the A atom $R_A$ versus the radius of the B atom $R_B$ for many $A_2BX_4$ compounds of known structure types and seeking heuristically simple, straight boundaries in the $R_A$ versus $R_B$ plane that best separate the domains of different structure types. The radii are sums $R_A = R_s(A) + R_p(A)$ of the quantum-mechanically calculated "orbital radii" $R_s(R_p)$, rather than empirical radii or phenomenological electronegativity scales. These success rates using first-principles orbital radii uniformly exceed the success rates using classic radii. Such maps afford a quick guess of the crystal structure of a yet unmade $A_2BX_4$ compound by placing its atomic orbital radii on such maps and reading off its structure type.**

## 1. Introduction

$A_2BX_4$ compounds[1–6] constitute a centrally important group in inorganic solid state, manifesting a wide range of physical phenomena including insulation, transparent conductivity, ferromagnetism, ferroelectricity, and superconductivity. The 790 known $A_2BX_4$ compounds[1–13] are distributed into 44 different crystal structure types as listed in Tables 1 and 2 (the Supporting Information lists the compounds belonging to each of the different structure types). This group of compounds exhibits significant chemical diversity, including chalcogen anions (X = O, S, Se, Te) as well as halides (X = F, Cl, Br, I), nitrides (X = N), cyanides (X = CN), and even nitrites ($X = NO_2$). The cations manifest cases where both A and B are main-group metals (A and B = Al, Mg, Ge, Sn) or cases where both A and B are transition elements (e.g., $Ni_2TiO_4$, $V_2MnO_4$) or cases where we have one of each (e.g., $Al_2NiO_4$) as well as rare-earth cationic species (e.g., $Yb_2FeS_4$). These compounds include cation-deficient structures (e.g., A-deficient $A_3B_2X_8$ or B-dificient $A_4BX_8$) as well as cases such as $A_3B_2X_6$ with cations in excess. The structures adopted by this group are no less fascinating than their chemical constitution. This family of compounds includes, for example, the spinel structure-type (255 members), the $Th_3P_4$ structure-type (87 members), the $Fe_2CaO_4$ structure-type (78 members), the $K_2SO_4$ structure-type (69 members), the $Cr_3S_4$ structure-type (57 members), and the Olivine ($Al_2BeO_4$) structure-type (48 members).[14] The $A_2BX_4$ structure-types differ in crystal classes (cubic, orthorhombic, rhombohedral) and local environments ("motifs"), covering tetrahedral and octahedral as well as 5- and 7-fold coordination sites.

An outstanding challenge in structural inorganic chemistry[2–4,6,15] and in solid-state physics[16,17] has been to explain the distribution of the known $A_2BX_4$ compounds into different structure types. Two leading types of approaches of predicting or rationalizing the crystal structure of a given $A_2BX_4$ compound have developed. In the deductive approach, one explicitly varies the structural degrees of freedom of an $A_2BX_4$ compound in search of a minimum of a given energy functional. In the inductive approach one offers a guess for the crystal structure of a given compound by analogy with the known structures of other compounds.

Most previous deductive approaches have focused on comparing a piece of the total (electronic + ionic) energy of different structures. The classical approach of crystal field stabilization energy (CFSE)[17] attempts to correlate the type of the observed local atomic structural motif (octahedral vs. tetrahedral) with the excess orbital energy resulting from the splitting of the *d*-like atomic orbital energies by the nonspherical crystal field. This approach is applicable only to the cases where A or B is open shell transition metal. Even for this restriction the method was typically applied only to a subset of the known cases that do contain open shell A or B atoms, for example, the 44 cases in Reference [17]. The predictive power of the method is rather low: 46% success. Similarly, the approach of comparing point-ion Madelung energies of different structures was tested only for a small (18 compounds[18]) part of the database. The success rate of distinguishing normal versus inverse spinels was 83%. Indeed, using the ion–ion contribution to the total energy of a solid has long been advocated as a useful criteria for qualitatively rationalizing the arrangements of certain ionic sublattices within complex multinary structures.[19] Another approach is the empirical valence force field[20] that minimizes the total energy of different

[*] Dr. X. Zhang, Dr. A. Zunger
National Renewable Energy Laboratory
Golden, Colorado, 80401 (USA)
E-mail: Alex_Zunger@nrel.gov

DOI: 10.1002/adfm.200901811

**Table 1.** Crystal structure types of $A_2BX_4$ compounds. The labels b1–b38 and d1, d3, and d9 of structures in the first column are taken from Wyckoff,[5] whereas labels S1–S3 indicate $Y_2CrS_4$-type, $Yb_3S_4$-type, and $Sr_2PbO_4$-type structures, respectively. The notation "none" refers to cases where no known Pearson symbol nor mineral name exists.

| Label | Prototype Compd. | Space Group | Pearson's Symbol/Mineral Name | No. of Compd. |
|---|---|---|---|---|
| b5 | $Al_2MgO_4$ | $Fd\bar{3}m$ ($O_h^7$) | cF56;Spinel | 255 |
| d9 | $Th_3P_4$ | $I\bar{4}3d$($T_d^6$) | none | 87 |
| b9 | $Fe_2CaO_4$ | $Pnma$($D_{2h}^{16}$) | none | 78 |
| b11 | $K_2SO_4$ | $Pnma$($D_{2h}^{16}$) | none | 69 |
| d3 | $Cr_3S_4$ | $C2/m$($C_{2h}^3$) | mC14 | 57 |
| b10 | $Al_2BeO_4$ | $Pnma$($D_{2h}^{16}$) | Olivine | 48 |
| b1 | $K_2MgF_4$ | $I4/mmm$($D_{4h}^{17}$) | none | 41 |
| b6 | $Mn_3O_4$ | $I4_1/amd$($D_{4h}^{19}$) | tI28;Hausmanite; distorted Spinel | 27 |
| b4 | $Ag_2HgI_4$ | $P\bar{4}2m$($D_{2d}^1$) | tI14;Thiogallate | 24 |
| b33 | $Li_2WO_4$ | $R\bar{3}$($C_{3i}^2$) | Phenakite | 14 |
| S1 | $Y_2CrS_4$ | $Pca2_1$($C_{2v}^5$) | none | 14 |
| S2 | $Yb_3S_4$ | $Pnma$($D_{2h}^{16}$) | none | 13 |
| d1 | $Pb_3O_4$ | $P4_2/mbc$($D_{4h}^{13}$) | none | 9 |
| b21 | $Al_2BaO_4$ | $P6_322$($D_6^6$) | none | 7 |
| S3 | $Sr_2PbO_4$ | $Pbam$($D_{2h}^9$) | none | 6 |
| b18 | $Na_2SO_4$ | $Fddd$($D_{2h}^{24}$) | Thenardite | 4 |
| b2 | $K_2PtCl_4$ | $P4/mmm$($D_{4h}^1$) | none | 3 |
| b3 | $K_2Pd(NO_2)_4$ | $P2_1/c$($C_{2h}^5$) | none | 2 |
| b7 | $Cr_2CuO_4$ | $I\bar{4}2d$($D_{2d}^{12}$) | distorted Spinel | 2 |
| b13 | $KHSO_4$ | $Pbca$($D_{2h}^{15}$) | none | 2 |
| b20 | $LiKSO_4$ | $P6_3$($C_6^6$) | none | 2 |
| b22 | $KNaSO_4$ | $P\bar{3}m1$($D_{3d}^3$) | Aphthitalite | 2 |

**Table 2.** Crystal structure types of $A_2BX_4$ compounds (continued from Table 1).

| Label | Prototype Compd. | Space Group | Pearson's Symbol/Mineral Name | No. of Compd. |
|---|---|---|---|---|
| b26 | $K_2SO_3(N_2O_2)$ | $Pnma$($D_{2h}^{16}$) | none | 2 |
| b30 | $Na(MoO_2)PO_4$ | $P2_1/c$($C_{2h}^5$) | none | 2 |
| b8 | $Ti_2CaO_4$ | $Cmcm$($D_{2h}^{17}$) | none | 1 |
| b12 | $Ba_2TiO_4$ | $P2_1/c$($C_{2h}^5$) | none | 1 |
| b14 | $H_2SO_4$ | $Cc$($C_s^4$) | none | 1 |
| b15 | $H_2SeO_4$ | $P2_12_12_1$($D_2^4$) | none | 1 |
| b16 | $Li_2SO_4$ | $P2_1/c$($C_{2h}^5$) | none | 1 |
| b17 | $Li_2SO_4$ (high-T) | $F\bar{4}3m$($T_d^2$) | none | 1 |
| b19 | $Na_2CrO_4$ | $Cmcm$($D_{2h}^{17}$) | none | 1 |
| b23 | $(NH_4)_2CrO_4$ | $Pm$($C_s^1$) | none | 1 |
| b24 | $Na_2S_2O_3$ | $P2_1/c$($C_{2h}^5$) | none | 1 |
| b25 | $(NH_4)_2S_2O_3$ | $C2/m$($C_{2h}^3$) | none | 1 |
| b27 | $BaHPO_4$ | $Pna2_1$($C_{2v}^9$) | none | 1 |
| b28 | $CaHPO_4$ | $P\bar{1}$($C_i^1$) | none | 1 |
| b29 | $NaBePO_4$ | $P2_1/c$($C_{2h}^5$) | none | 1 |
| b31 | $NaH(PO_3NH_2)$ | $P6_3$($C_6^6$) | none | 1 |
| b32 | $K(UO_2)VO_4$ | $P2_1/c$($C_{2h}^5$) | none | 1 |
| b34 | $Bi_2PbS_4$ | $Pnma$($D_{2h}^{16}$) | Galenobismuthite | 1 |
| b35 | $Sb_2FeS_4$ | $Pnma$($D_{2h}^{16}$) | oP28;Berthierite | 1 |
| b36 | $As_2PbS_4$ | $P2_1/c$($C_{2h}^5$) | Scleroclase | 1 |
| b37 | $Sb_2SnTe_4$ | $R\bar{3}m$($D_{3d}^5$) | hR7; | 1 |
| b38 | $In_2ZnS_4$ | $R3m$($C_{3v}^5$) | hP14; | 1 |
| Total | | | | 790 |

competing structures from empirically parametrized interatomic potential functions. This approach too, relies on selecting certain pieces of the full ion + electron total energy and on specific, approximate analytic forms of the potential terms. This approach has been applied[20] to a very restricted number of cases (54 compounds), predicting correctly 45 compounds (or 83% success).

Instead of minimizing pre-selected pieces of the full total-energy, one might of course attempt to minimize an all-inclusive total energy expression, such as the density-functional and Hartree–Fock expressions. The density-functional calculations of the total energy were done by Marinelli et al. for $In_2MgS_4$,[16] Warren et al. and Thibaudeau et al. for $Al_2MgO_4$,[21] and Wei et al. for 18 spinel compounds.[22] The Hartree–Fock calculations of the total energy were done by Catti et al. for $M_2CrO_4$ (M = Mg, Mn, Zn) and Mitchell et al. for $M_2ZnO_4$ (M = Al, Fe).[23] Seko et al. used the cluster expansion method combined with density-functional calculations to investigate the ground state structures of 6 spinel compounds.[24] This successful deductive approach, however, is not easily applicable to large databases, works on a case by case basis, and requires optimization of the total energy with respect to all crystallographic parameters of each structure type. At this point most studies have applied such procedures by fixing the lattice-type (e.g., the lattice vectors were fixed at the outset as monoclinic or orthorhombic) and optimizing the total energy only with respect to cell-internal atomic positions and the magnitude of the lattice vectors. Such approaches do not determine the full structure type. Generalization to Global Space Group Optimization (GSGO)[25] is however possible.

An alternative approach to minimization of the total energy is based on diagrammatic sorting of compounds.[6,26–32] In this inductive approach one constructs coordinates $R_1$(A,B) and $R_2$(A,B) based on some properties of the A and B atoms, and searches in a $R_1$ versus $R_2$ map for simple connected regions in which unique structure types are confined. The borderlines between different structure-types in the $R_1$ versus $R_2$ plane are constructed pragmatically so as to affect the best separation of the structures.

A critical aspect of diagrammatic separation is the need to apply it to as complete a data set as possible without preselection. The choice of atomic-scale coordinates can vary and in the past was often related to the data base of structures considered. Mooser and Pearson[26] tried in 1959 to separate fourfold coordinated binary AB solids from sixfold coordinated ones, considering the difference in electronegativity $R_1 = \chi_A - \chi_B$ and the average of principal quantum number $R_2 = (n_A + n_B)/2$. Their data base had ~120 compounds (80% of the total data base[30]) in 4 structure types and the success rate was 95%. Miedema et al.[27] separated compounds forming from phase-separating binary A–B metal alloys based on relative atomic size and relative work-function. Applying the same Miedema coordinates to separation of structure types of binary AB compounds[30] was generally unsuccessful. Muller and Roy[6] considered in 1974 the $A_2BX_4$ (X = O, S) group of ~250 compounds in 13 structure types where ~200 compounds were not included.[33] The coordinates they selected were $R_1 = r_A$ and $R_2 = r_B$, where $r_A$ and $r_B$ are the crystal radii of A and B ions (using supplemented[6] Shannon–Prewitt crystal radii[34]). They obtained a success rate of 96%. Bloch and co-workers[28] and Phillips and Chelikowsky[29] suggested the use of angular momentum dependent coordinates, and used successfully the quantum-defect coordinates determined from atomic spectral data. They applied it to distinguish the most stable crystal structures of 34 non-transition elemental solids and 59 octet AB binary compounds[28] (53% of the total data base[30]). In 1984, Pettifor[31] advanced atomic scale coordinates $R_A$ and $R_B$ that were pure numbers assigned to each element in the Periodic Table with the sole purpose of obtaining the maximum statistical structure separation in the $R_1$ versus $R_2$ plane, considering all known binary AB compounds in 34 different structure types. In 2001, Villars et al.[32] constructed the coordinates by optimizing nonlinear expressions of Pettifor's numbers[31] and other atomic scales with the sole target of maximum statistical separation, resulting in very complicated coordinates. Pettifor's numbers[31] were not applied to $A_2BX_4$ compounds (but will be below). In the present work, we will use the broadest list of $A_2BX_4$ compounds and structures and apply the quantum-mechanical orbital radii,[35] reviewed next. The results will be compared to those we find with other literature radii.

## 2. First-Principles Atomic Orbital Radii

Zunger and co-workers[35,36] proposed the first-principles pseudopotential orbital radii concept. The idea was to i) define atomic radii from a microscopic theory of the free-atoms and ii) extract atomic coordinates that have the characteristic size of atomic cores and thus are free from the need[34,37] to specify atomic-radii that depend on a multitude of valence chemical factors, such as solid-state coordination number (leading to tetrahedral vs. octahedral radii); oxidation number, etc. Indeed, such detailed dependencies (while important for defining radii from crystallography) can lead to a proliferation of diagrammatic maps. To construct core-radii from an electronic structure theory, Zunger[30] utilized the pseudopotential concept.[38] The core + valence ("all-electron") Schrödinger equation for free-atoms which treats core and valence electrons on the same footing reads

$$\left\{-\frac{1}{2}\nabla^2 + V_{\text{e-ion}}^{(c+v)} + V_{\text{e-e}}^{(c+v)}[\rho]\right\}\psi_{\text{nl}} = \varepsilon_{\text{nl}}\psi_{\text{nl}}. \quad (1)$$

It contains an electron-ion $V_{\text{e-ion}}^{(c+v)} = -(Z_c + Z_v)/r$ term (due to core and valence charges $Z_c$ and $Z_v$, respectively) and an all-electron screening $V_{\text{e-e}}^{(c+v)}[\rho]$, which is the inter-electronic Hartree exchange and correlation terms due to the core + valence electron charge-density $\rho = \sum_{\text{nl}}^{c+v} |\psi_{\text{nl}}|^2$. One knows heuristically that information on structural preferences and chemical reactivity is encoded primarily in the valence orbitals yet the (core + valence) orthogonality principle does not permit one to solve Eq. (1) just for the chemically significant valence orbitals. (For example, a direct solution for the 3s orbital of Na without reference to the 1s + 2s core would inevitably cause the 3*s* to lose its 2 nodes and collapse into a 1s state). Such a collapse can be rigorously prevented by formulating an additional term in the effective potential, replacing Eq. (1) by a valence-only (pseudo) Schrödinger equation

$$\left\{-\frac{1}{2}\nabla^2 + V_{\text{ps}}^{(l)} + V_{\text{e-ion}}^{(v)} + V_{\text{e-e}}^{(v)}[n]\right\}\chi_{\text{nl}} = \varepsilon_{\text{nl}}\chi_{\text{nl}}, \quad (2)$$

where $V_{e-ion}^{(v)} = -Z_v/r$ is the valence-only electron-ion attraction, $\chi_{nl}$ are nodeless valence (pseudo) orbitals, and $V_{e-e}^{(v)}[n]$ is the screening supplied by valence pseudo orbitals $n = \sum_{nl}^{v} |\chi_{nl}|^2$. In Eq. (2), $V_{ps}^{(l)}$ is an angular-momentum ($l$) dependent core potential to be determined by requiring that the valence orbital energies $\{\varepsilon_{nl}\}$ of the all-electron Eq. (1) match those of Eq. (2), and that the nodeless valence pseudo-orbitals $\{\chi_{nl}\}$ match some significant aspects (see below) of the real valence orbitals $\left\{\psi_{nl}^{(v)}\right\}$ of Eq. (1). There are a number of ways to enforce the latter condition.[38,39] One possibility is to create "norm-conservation," that is, to force $\chi_{nl}(r)$ to match exactly $\psi_{nl}^{(v)}(r)$ in the tail region and solve for $V_{ps}^{(l)}$ that does so. A simpler and in our view more elegant approach is to describe the valence pseudo orbital $\chi_{nl}$ as a rotation in the space of the core + valence all-electron orbitals[35,36] $\psi_{nl}$

$$\chi_{nl}^{(v)}(r) = \sum_{n'l'}^{c+v} C_{nl,n'l'} \psi_{n'l'}^{(c+v)}(r) \tag{3}$$

The choice of wave-function transformation coefficients[36] is based simply on maximizing the similarity between the true and pseudo-orbitals [see Eq. (3)] with a minimum core amplitude, subject to the constraints that pseudo-orbitals be normalized and nodeless.[40] Once $\{\chi_{nl}\}$ was formulated from Eq. (3), the pseudopotential $V_{ps}^{(l)}(r)$ was obtained by substituting Eq. (3) into Eq. (2) and solving Eq. (2) to find $V_{ps}^{(l)}(r)$. This was carried out in 1978[35,36] using the density-functional formalism for describing the inter-electronic interaction, $V_{e-e}[\rho]$ and $V_{e-e}[n]$.

Pseudopotentials $\{V_{ps}^{(l)}(r)\}$ were originally derived for simplifying core + valence calculations of solids. But it became clear[30] that if they are constructed systematically [e.g., via requiring Eq. (3)] they exhibit interesting chemical regularities that might be exploited. For example, these first-principles pseudopotentials[35,36] $\{V_{ps}^{(l)}(r)\}$ revealed a natural, $l$-dependent atomic size directly from atomic physics [Eqs. (1) and (2)], not from measured interatomic distances in solids (Figs. 1–4 in Ref. [36] demonstrate these chemical trends in orbital radii along the Periodic Table). Zunger[30] selected the classical tuning point $V(R_l) = 0$ as the definition of the orbital radii $R_s$, $R_p$, and $R_d$, where $V$ was taken as the total effective potential seen by a valence orbital of angular momentum $l$, that is, $V = V_{ps}^{(l)} + V_{e-ion}^{(v)} + V_{e-e}^{(v)}[n]$. These radii were tabulated for 70 elements in the Periodic Table.[30] They showed interesting trends along rows and columns of the Periodic Table (see Fig. 6 in Ref. [36]), decreasing from left to right along rows and increasing dramatically from top to bottom along columns. Also, the orbital radii showed[41] an interesting relationship to a few classic chemical scales. For example, i) the first-principles p-orbital radii correlate with the empirical ("empty core") pseudopotential radii determined earlier for metals (Fig. 8 in Ref. [41]), ii) the reciprocal first-principles orbital radii $1/R_l$ correlate with the measured multiplet-averaged ionization energies of the elements (Figs. 10 and 11 in Ref. [41]), iii) the first-principles s-orbital atomic radii $R_s$ correlate with averaged outer node positions of the atomic wavefunctions (Figs. 13 and 14 in Ref. [41]) and with Pauling's tetrahedral radii (Fig. 15 in Ref. [41]), iv) the combined $R_\sigma = R_s + R_p$ radii correlate with Pauling's univalent radii (Fig. 16 in Ref. [41]). Similar correlations exist with respect to reciprocal shielding constants $1/Z_s^*$ (Fig. 18 in Ref. [41]).

The first-principles orbital radii of Zunger were used in 1978 to systematize the crystal structures of 565 binary octet AB and non-octet compounds in 34 different structure types,[30] as well as to organize the first-principles total energies of Wurtzite versus Zincblend.[42] Burdett and co-workers[2] used Zunger's orbital radii[30] for numerous problems in inorganic chemistry. Villars and co-workers[43] examined the statistical rate of success of a large number of elemental coordinates in affecting structural predictions of diagrammatic separation maps and concluded that the best structural sorting is achieved by Zunger's first principles orbital radii, along with the average electron-per-atom ratio and the Martynov–Batsanov electronegativity.

In this paper we use the pseudopotential orbital radii[30] $R_s$ and $R_p$ to generate the dual coordinates

$$R_A = R_s(A) + R_p(A) \tag{4a}$$

$$R_B = R_s(B) + R_p(B) \tag{4b}$$

to construct diagrammatic separation maps for $A_2BX_4$ compounds, where $R_s$ and $R_p$ are the orbital radii from Table 1 in Reference [30].

## 3. Orbital Radii Structure-Field Maps of $A_2BX_4$ Compounds

### 3.1. General Description

Our maps include 688 compounds out of the total 790 listed in Tables 1 and 2 (see also Supporting Information). The compounds excluded include the following cases: i) compounds containing U (5 cases), Th (one case), and H (2 cases) whose orbital radii were not determined, ii) compounds like $(Fe,Mg)_2SiO_4$ (93 cases), which contain chemical groups for either A or B in $A_2BX_4$ and cannot be represented by two indices of Eq. (4), and iii) the high temperature form of $Li_2SO_4$ in one-membered group b17 (one case).

Figure 1 shows the orbital radii structure-field map for 266 oxides and Figure 2 shows those for 219 sulfides, 132 selenides, and 31 tellurides. There are 40 $A_2BX_4$ compounds with other anions: 15 fluorides, 10 chlorides, 2 bromides, 2 iodides, 2 nitrides, 7 cyanides, and 2 nitrites. Their orbital radii structure-field maps have no errors. Out of a total 688 compounds, we find a total of 17 errors. The success rate is 98%. The errors are explicitly listed in Table 3, and are discussed next.

### 3.2. Misplaced Compounds

There are three types of errors. First, we find 6 cases in which the experimentally reported structure is a high-temperature phase but the low-temperature structure is not reported, so that the conflict with the orbital radii approach (that predicts the most stable structure at $T = 0$) is not necessarily a contradiction. Second, another type of error is the one-membered group. This compound ($Pb_2SO_4$) could be defined as occupying a space of its own, so that

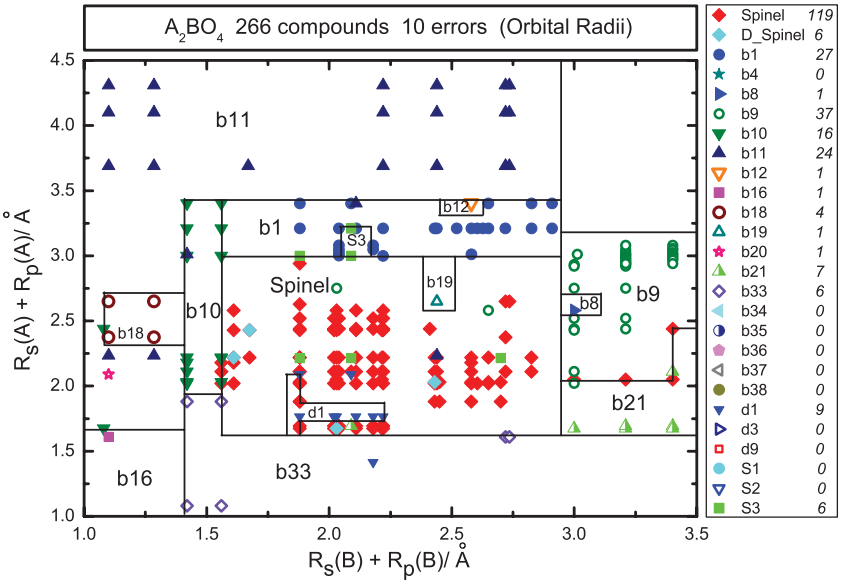


**Figure 1.** Orbital radii structure-field map of $A_2BO_4$. Since b6 and b7 (Table 1) are distorted spinel structure types, they are included in the type of "spinel." The orbital radii of the Ln elements (Ce to Lu) are obtained by linear interpolation between La and Hf.

the conflict with the orbital radii approach is also not necessarily a contradiction. Third, ten cases are true errors. $Cd_2PbO_4$, $Cd_2PtO_4$, $Cd_2SnO_4$, $Ga_2PbO_4$, $Pb_3O_4$, $Tl_2CrO_4$, $Sc_2MgO_4$, and $Ti_2NaO_4$ were determined experimentally to exist in S3,[6] S3,[6] S3,[13] b21,[5] d1,[5] b11,[5] b9,[12] and b9[12] structures (see Supporting Information), respectively, but appear in the map in the spinel (b5) region. $As_2NiO_4$ has the d1 structure,[5] but is placed in the map in the region of b33. $Ni_2RhS_4$ is reported to exist in the spinel structure,[6] while its orbital radii place it inside the d3 region. The spinel and d3 structures (see Figs. S1 and S5 in the Supporting Information) are closely related: both have their 2/3 cations octahedrally coordinated; their anion sub-lattices (fcc in spinel and hcp in d3, both slightly distorted) are very similar.

The compounds on the borderlines in the orbital radii structure-field maps shown above (Figs. 1 and 2) may be susceptible to conversion to the alternative structure types. For example, $Ca_2GeO_4$ is on the borderline of b10 versus b1, $Mg_2GeO_4$ is on the borderline of b10 versus b5, $Li_2MoO_4$ and $Zn_2GeO_4$ are on the borderline of b33 versus b5, $Al_2CdS_4$ is on the borderline of b4 versus b5, and $Cr_2CoS_4$, $Cr_2FeS_4$, $Cr_2MnS_4$ and $V_2CuS_4$ are on the borderline of b5 versus d3. These compounds were found to manifest the corresponding pressure-induced structural transformations[6] between the structures at the borderlines.

The orbital radii structure-field maps shown above are specific to each anion: Figure 1 is for X = O, Figure 2a is for X = S, and so on. If we included all compounds with all anion types in a single map ("all-anion map"), we find (see Fig. S9 in the Supporting Information) a success rate of only 84%. This means that the diagrammatical separation of the structure types is anion-dependent.

If we include $R_d$ in the indices, that is, $R_A = R_s(A) + R_p(A) + R_d(A)$ and $R_B = R_s(B) + R_p(B) + R_d(B)$, the structure-field maps do not increase the success rate. This might suggest that the *explicit* role of $R_d$ in determining the crystal of $A_2BX_4$ is minor. Recall, however, that all valence electrons, including s + p + d affect the radii through the screening $V_{e-e}^{(v)}[n]$.

## 4. Orbital Radii Maps Separating Normal versus Inverse $A_2BX_4$ Spinels

The orbital radii approach was further used to sort the spinels, the major group of the $A_2BX_4$ compounds, into normal and inverse spinels.[2] In the spinel structure, the anions form a (slightly distorted) fcc sub-lattice. In the primitive-cell, there are (symmetrically-equivalent) 8 anionic sites, 2 tetrahedral cationic sites ($T_1$ and $T_2$), and 4 octahedral cationic sites ($O_1$, $O_2$, $O_3$, $O_4$). Normal spinel is a single structure type $(O_1^AO_2^AO_3^AO_4^A)(T_1^BT_2^B)X_8$, with A occupying all four octahedral sites, and B occupying the two tetrahedral sites. Inverse spinels are a class of structures $(O_1^{A/B}O_2^{A/B}O_3^{A/B}O_4^{A/B})$ $(T_1^AT_2^A)X_8$, where A occupies deterministically the two tetrahedral sites, but the four octahedral sites $O_1$, $O_2$, $O_3$, $O_4$ can be occupied each either by A or B. This gives rise to a large set of configurations.

Numerous attempts were made to predict the cation distribution in the spinels. These include the CFSE method[17] with less than 50% success rate even when applied only to transition metal cations. Another approach is using the Madelung energy,[18] applied only to 18 compounds with 83% success. Burdett et al.[2] used Zunger's orbital radii to separate normal versus inverse spinels with 98% success rate, however, with a smaller database [172 spinels out of 284 known spinels (see Table 1)].

Figure 3 shows the all-anion orbital radii maps for normal versus inverse spinels. The b6 and b7 compounds (distorted spinels, see Table 1) are included. Our map includes 230 compounds out of the total 284. The compounds excluded include the following cases: i) compounds (30 cases) like $AlFeNiO_4$, which cannot be represented by two indices and ii) cation-deficient and cation-excess spinels (24 cases) whose cationic sites are not regularly occupied.

Out of 230 spinel compounds, we find 10 errors, which are listed in Table 4. The success rate is 96%. Compared to Burdett's (all-anion) map,[2] our map has 6 more errors (5 halides and 1 $A_3B_4$-type) because we included all the known spinels that can be included. If we plot a separation map of cation distribution in spinels for each anion-type (separate-anion maps), the success rate is 98%, which is slightly higher than the success rate of the all-anion map (96%). This indicates that the anion type plays a very minor role in determining the cation distribution in spinels. If we include $R_d$ in the indices, the success rates of the all-anion map and separate-anion maps do not increase. This might suggest that the explicit role of $R_d$ in determining the cation distribution in spinels is minor.

## 5. Comparison with Other Radii

We constructed the separation maps using Shannon's crystal radii,[37] $R_1 = r_A$ and $R_2 = r_B$, where $r_A$ and $r_B$ are the crystal radii of

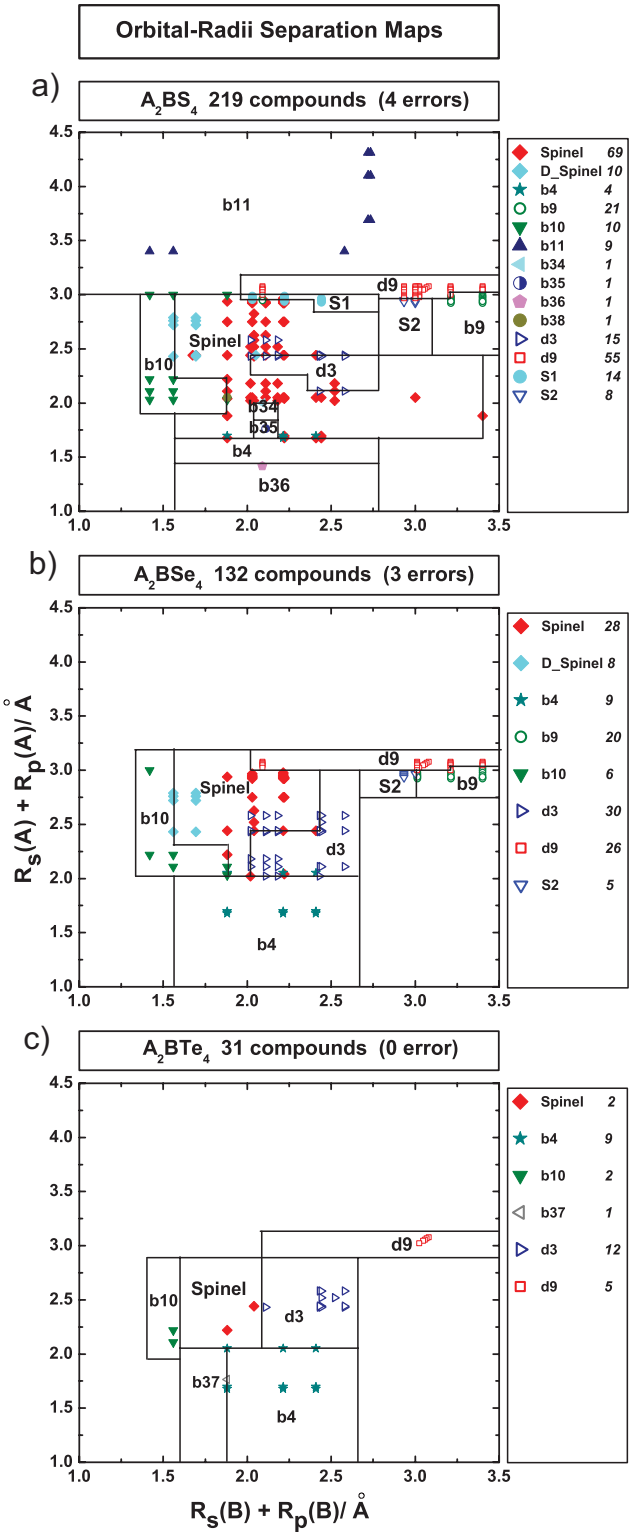


**Figure 2.** Orbital radii structure-field maps of a) $A_2BS_4$, b) $A_2BSe_4$, and c) $A_2BTe_4$.

**Table 3.** List of compounds that, according to their orbital radii, appear in the sorting map in a different structure than that designated for them by experimental assessments.

| Compound | Experimentally Assigned Structure | Orbital Map Structure |
|---|---|---|
| $Ti_2CoS_4$ | d3 (high temperature) [a] | spinel (b5) |
| $Ti_2FeS_4$ | d3 (high temperature) [a] | spinel (b5) |
| $Ti_2NiS_4$ | d3 (high temperature) [a] | spinel (b5) |
| $Ti_2CoSe_4$ | d3 (high temperature) [a] | spinel (b5) |
| $Ti_2FeSe_4$ | d3 (high temperature) [a] | spinel (b5) |
| $Ti_2NiSe_4$ | d3 (high temperature) [a] | spinel (b5) |
| $Pb_2SO_4$ | b20 (one member in the map) [b] | b11 |
| $Cd_2PbO_4$ | S3 [c] | spinel (b5) |
| $Cd_2PtO_4$ | S3 [c] | spinel (b5) |
| $Cd_2SnO_4$ | S3 [d] | spinel (b5) |
| $Ga_2PbO_4$ | b21 [b] | spinel (b5) |
| $Pb_3O_4$ | d1 [b] | spinel (b5) |
| $Tl_2CrO_4$ | b11 [b] | spinel (b5) |
| $Sc_2MgO_4$ | b9 [e] | spinel (b5) |
| $Ti_2NaO_4$ | b9 [e] | spinel (b5) |
| $As_2NiO_4$ | d1 [b] | b33 |
| $Ni_2RhS_4$ | spinel (b5) [c] | d3 |

[a] Reference [9]. [b] Reference [5]. [c] Reference [6]. [d] Reference [13]. [e] Reference [12].

A and B ions,[37] including every compound that can be included. There are 40 compounds that are included in orbital radii maps but cannot be included in Shannon's radii maps (see Supporting Information). The 5 compounds containing U (not included in orbital radii maps) are included in Shannon's radii maps. The success rates of the structure-field maps and cation-distribution map using Shannon's crystal radii[37] (see Figs. S10 and S11 in the Supporting Information) are 92% and 74% compared to the success rates of the orbital radii maps at 98% and 96%, respectively. Shannon's radii[37] were revised slightly from Shannon–Prewitt crystal radii[34] in 1976. Before that, Muller and Roy[6] had

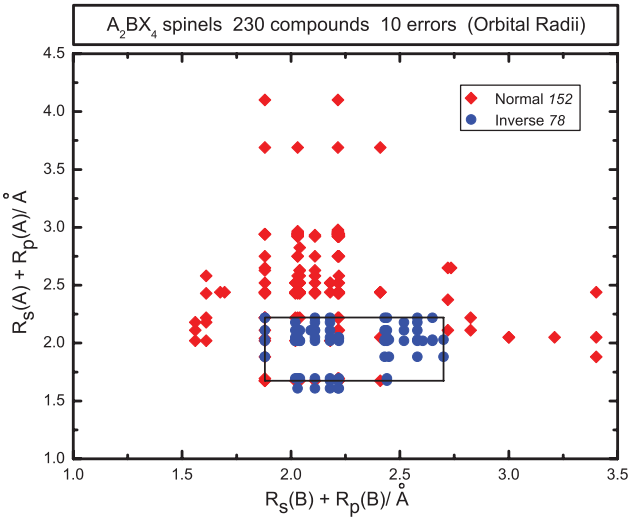


**Figure 3.** Diagrammatic separation map of $A_2BX_4$ spinels (all-anion) for cation distribution (i.e., normal vs. inverse spinels) using orbital radii [30].

**Table 4.** List of spinel compounds that, according to their orbital radii, appear in the sorting map in a different cation distribution than that designated for them by experimental assessments.

| Compound | Experimentally Assigned Cation Distribution | Orbital Map Cation Distribution |
|---|---|---|
| $Fe_2CdO_4$ | Normal [a] | Inverse |
| $Fe_2MnO_4$ | Normal [a] | Inverse |
| $Co_2NiS_4$ | Normal [a] | Inverse |
| $In_2HgS_4$ | Normal [a] | Inverse |
| $Li_2NiF_4$ | Inverse [b] | Normal |
| $Li_2CdCl_4$ | Inverse [a] | Normal |
| $Li_2FeCl_4$ | Inverse [a] | Normal |
| $Li_2MgCl_4$ | Inverse [a] | Normal |
| $Li_2MnCl_4$ | Inverse [a] | Normal |
| $Co_3O_4$ | Normal [a] | Inverse |

[a] Reference [6]. [b] Reference [5].

supplemented Shannon–Prewitt radii.[34] The separation maps using supplemented Shannon–Prewitt radii[6,34] are similar and have similar success rates with the above maps using Shannon's crystal radii.[37]

We tested Pauling's univalent crystal radii[44] as indices, that is, $R_1 = r^{univ}(A)$ and $R_2 = r^{univ}(B)$ where $r^{univ}(A)$ and $r^{univ}(B)$ were given in Reference [44]. Only 42% of the total database can be included in the structure-field maps (since the univalent crystal radii for Fe, Co, Ni, Rh, and so on, are not tabulated in Ref. [44]) and the success rate is 77%; only 40% of spinels can be included in the cation-distribution map with a success rate 82%. Trying separation maps for the same sets of compounds but using orbital radii, we obtained success rates of 98% and 96% for structure types and cation distribution, respectively.

We also tested Pauling's covalent radii[45] as coordinates, that is, $R_1 = r^{cov}(A)$ and $R_2 = r^{cov}(B)$ where $r^{cov}(A)$ and $r^{cov}(B)$ are the covalent radii of A and B atoms.[45] Only 22% of the total database can be included (since for many elements covalent radii were not tabulated in Ref. [45]) in the structure-field maps with a success rate of 85% and only 32% of spinels can be included in the cation-distribution map with a success rate of 74%. Trying orbital radii maps for the same sets of compounds, we obtained success rates of 93% for structure types and 96% for cation distribution.

Finally, we tested Pettifor's numbers[31] $R_1 = \chi(A)$ and $R_2 = \chi(B)$ where $\chi(A)$ and $\chi(B)$ were the given numbers in Reference [31]. The success rates for structure types and cation distribution in spinels using Pettifor's numbers[31] (see Fig. S12 in the Supporting Information) are 91% and 80%.

In summary, we list in Table 5 the number of compounds and number of errors in the structure-field maps of oxides (Fig. 1), sulfides + selenides + tellurides (Fig. 2), and other anions (halides + nitrides + cyanides + nitrites), as well as cation-distribution maps (all-anion, Fig. 3) using orbital radii, Shannon's crystal radii, Pauling's univalent crystal radii, Pauling's covalent radii, and Pettifor's numbers as indices. We can see from Table 5 that the orbital radii maps give the best separation of structure types and normal versus inverse spinels. The diagrammatic separation method using orbital radii can also be applied to other families of ternary or quaternary compounds.

## 6. Conclusions

It is demonstrated that the nonlocal pseudopotential orbital radii, $R_s$ and $R_p$, are capable of systematizing and predicting the crystal structures of $A_2BX_4$ compounds with a success rate of 98%. The separation of the structure types is anion-dependent. While the fact that anion-independent coordinates are good enough to predict the correct cation distribution in spinels with 96% success demonstrates that the anion type plays a minor role in determining normal versus inverse spinels. The d-orbital radii are of no explicit importance in determining the crystal structure, and even the cation distribution in spinels. Separation maps using other radii

**Table 5.** Type of diagrammatic separation maps for $A_2BX_4$ compounds and their success rates.

| Type of Coordinate | Type of Map | No. of Compd. | No. of Errors | Success Rates |
|---|---|---|---|---|
| Zunger's orbital radii[30] | Oxides | 266 | 10 | |
| | S + Se + Te | 382 | 7 | 98% |
| | other-X | 40 | 0 | |
| | N *vs* I | 230 | 10 | 96% |
| Shannon's crystal radii[37] | Oxides | 256 | 23 | |
| | S + Se + Te | 357 | 27 | 92% |
| | other-X | 40 | 0 | |
| | N *vs* I | 212 | 56 | 74% |
| Pauling's univalent crystal radii[44] | Oxides | 150 | 45 | |
| | S + Se + Te | 156 | 31 | 77% |
| | other-X | 27 | 0 | |
| | N *vs* I | 114 | 20 | 82% |
| Pauling's covalent radii[45] | Oxides | 84 | 13 | |
| | S + Se + Te | 87 | 13 | 85% |
| | other-X | 3 | 0 | |
| | N *vs* I | 92 | 24 | 74% |
| Pettifor's Numbers[31] | Oxides | 266 | 24 | |
| | S + Se + Te | 382 | 39 | 91% |
| | other-X | 40 | 0 | |
| | N *vs* I | 230 | 45 | 80% |

are also studied to compare with the orbital radii maps. Their success rates are lower than those of the orbital radii maps.

## Acknowledgements

AZ wishes to thank Iris Inbar who contributed greatly in the early stages of this work. We thank Mayeul d'Avezac, Thomas O. Mason, and Kenneth R. Poeppelmeier for useful discussions. Research supported by the U.S. Department of Energy, Office of Basic Sciences, Division of Materials Sciences and Engineering, Energy Frontier Research Centers, under Award No. DE-AC36-08GO28308 to NREL. Supporting Information is available online from Wiley InterScience or from the author.

Received: September 25, 2009
Revised: January 26, 2010
Published online: May 18, 2010

**Note added in proof:** We have recently examined the cases (Table 3) where orbital radii (OR) maps make a different structure assignment (S-OR) than the experimentally assigned structure (S-Expt) by computing the total-energies of S-OR and S-Expt structures via spin-polarized DFT. We find that 4 out of the 17 errors are probably not real errors, because $E_{DFT}$(S-OR) < $E_{DFT}$(S-Expt). This is the case for $Ti_2NiS_4$, $Cd_2PbO_4$, $Cd_2SnO_4$, and $Sc_2MgO_4$. For the remaining compounds in Table 3, $E_{DFT}$(S-OR) > $E_{DFT}$(S-Expt). $Ti_2NiSe_4$ is hardly different in both structures with an energy difference of ~0.01 eV per atom. More details will be published in future DFT paper by X. Zhang, V. Stevanović, and A. Zunger.

[1] P. Villars, L. D. Calvert, *Pearson's Handbook of Crystallographic Data for Intermetallic Phases*, ASM International, Materials Park, OH **1991**.
[2] a) J. K. Burdett, G. D. Price, S. L. Price, *Phys. Rev. B* **1981**, *24*, 2903. b) J. K. Burdett, G. D. Price, S. L. Price, *J. Am. Chem. Soc.* **1982**, *104*, 92.
[3] J. K. Burdett, *Chemical Bonding in Solids*, Oxford University Press, Oxford **1995**.
[4] R. J. Hill, J. R. Craig, G. V. Gibbs, *Phys. Chem. Miner.* **1979**, *4*, 317.
[5] R. W. G. Wyckoff, *Crystal Structures*, Vol. *2* and Vol. *3*, Robert E. Krieger Publishing Company, Malabar, Florida **1981**, [Structure types d1, d3, d9 are from Vol. 2; Structure types b1-b38 are from Vol. 3.]
[6] O. Muller, R. Roy, *The Major Ternary Structural Families*, Springer-Verlag, Berlin **1974**.
[7] D. Mandrus, V. Keppens, B. C. Chakoumakos, *Mater. Res. Bull.* **1999**, *34*, 1013.
[8] C. Q. Feng, L. Li, Z. P. Guo, D. Q. Shi, R. Zeng, X. J. Zhu, *J. Alloys Compd.* **2009**, *478*, 767.
[9] a) A. T. Burkov, T. Nakama, M. Hedo, K. Shintani, K. Yagasaki, N. Matsumoto, S. Nagata, *Phys. Rev. B* **2000**, *61*, 10049. b) V. Abadie, S. Jobic, R. Krachler, H. Ipser, I. Orion, R. Brec, *J. Alloys Compd.* **1998**, *268*, 50. c) Q. Wang, N. Evans, S. M. Zakeeruddin, I. Exnar, M. Grätzel, *J. Am. Chem. Soc.* **2007**, *129*, 3163. d) H. Weng, Y. Kawazoe, X. Wan, J. Dong, *Phys. Rev. B* **2006**, *74*, 205112. e) R. H. Plovnick, M. Vlasse, A. Wold, *Inorg. Chem.* **1968**, *7*, 127.
[10] J. V. Ibarra, C. Cilleruelo, E. Garcia, M. Pineda, J. M. Palacios, *Vib. Spectrosc.* **1998**, *16*, 1.
[11] P. Lombard, B. Boizot, N. Ollier, A. Jouini, A. Yoshikawa, *J. Cryst. Growth* **2009**, *311*, 899.
[12] a) M. Shizuya, M. Isobe, E. Takayama-Muromachi, *J. Solid State Chem.* **2007**, *180*, 2550. b) H. Müller-Buschbaum, *Z. Anorg. Allg. Chem.* **1966**, *343*, 113.
[13] T. O. Mason, D. R. Kammler, B. J. Ingram, G. B. Gonzalez, D. L. Young, T. J. Coutts, *Thin Solid Films* **2003**, *445*, 186.
[14] Yet, some $A_2BX_4$ structure types are populated in nature just by a few chemical compounds such as the last 20 structure-types listed in Tables 1 and 2.
[15] a) P. A. Cox, *Transition Metal Oxides*, Clarendon Press, Oxford **1992**. b) C. N. R. Rao, B. Raveau, *Transition Metal Oxides*, VCH Publishers, Weinheim, Germany **1995**.
[16] a) M. Marinelli, S. Baroni, F. Meloni, *Phys. Rev. B* **1988**, *38*, 8258. b) M. Marinelli, T. M. de Pascale, F. Meloni, G. Mula, M. Serra, S. Baroni, *Phys. Rev. B* **1989**, *40*, 1725.
[17] a) J. D. Dunitz, L. E. Orgel, *J. Phys. Chem. Solids* **1957**, *3*, 318. b) D. S. McClure, *J. Phys. Chem. Solids* **1957**, *3*, 311.
[18] a) V. S. Urusov, *Cryst. Res. Technol.* **1981**, *16*, K62. b) C. Glidewell, *Inorg. Chim. Acta* **1976**, *19*, L45. c) A. N. Cormack, G. V. Lewis, S. C. Parker, C. R. A. Catlow, *J. Phys. Chem. Solids* **1988**, *49*, 53. d) V. M. Talanov, L. A. Frolova, *Inorg. Mater.* **1982**, *18*, 1380. e) M. Matsui, W. R. Busing, *Phys. Chem. Miner.* **1984**, *11*, 55.
[19] a) R. Hoppe, in *Crystal Structure and Chemical Bonding in Inorganic Chemistry* (Eds: C. J. M. Rooymans, A. Rabenau), Elsevier, New York **1975**, *pp. 127*. b) R. Hoppe, *Angew. Chem. Int. Ed.* **1966**, *5*, 95. c) R. Hoppe, *Z. Naturforsch. A* **1995**, *50*, 555.
[20] S. A. Kutolin, V. P. Tishchenko, V. I. Kotyukov, N. L. Kotlevskaya, *Inorg. Mater.* **1987**, *23*, 268.
[21] a) M. C. Warren, M. T. Dove, S. A. T. Redfern, *J. Phys.: Condens. Matter* **2000**, *12*, L43. b) P. Thibaudeau, A. Debernardi, V. T. Phuoc, S. da Rocha, F. Gervais, *Phys. Rev. B* **2006**, *73*, 064305.
[22] S.-H. Wei, S. B. Zhang, *Phys. Rev. B* **2001**, *63*, 045112.
[23] a) M. Catti, F. F. Fava, C. Zicovich, R. Dovesi, *Phys. Chem. Miner.* **1999**, *26*, 389. b) D. W. Mitchell, T. P. Das, W. Potzel, W. Schiessl, H. Karzel, M. Steiner, M. Köfferlein, U. Hiller, G. M. Kalvius, A. Martin, W. Schäfer, G. Will, I. Halevy, J. Gal, *Phys. Rev. B* **1996**, *53*, 7684.
[24] a) A. Seko, K. Yuge, F. Oba, A. Kuwabara, I. Tanaka, T. Yamamoto, *Phys. Rev. B* **2006**, *73*, 094116. b) A. Seko, K. Yuge, F. Oba, A. Kuwabara, I. Tanaka, *Phys. Rev. B* **2006**, *73*, 184117.
[25] a) D. M. Deaven, K. M. Ho, *Phys. Rev. Lett.* **1995**, *75*, 288. b) N. L. Abraham, M. I. J. Probert, *Phys. Rev. B* **2006**, *73*, 224104. c) A. R. Oganov, C. W. Glass, *J. Chem. Phys.* **2006**, *124*, 244704. d) G. Trimarchi, A. Zunger, *Phys. Rev. B* **2007**, *75*, 104113. e) G. Trimarchi, A. Zunger, *J. Phys.: Condens. Matter* **2008**, *20*, 295212.
[26] a) E. Mooser, W. B. Peasron, *Acta Crystallogr.* **1959**, *12*, 1015. b) W. B. Pearson, *J. Phys. Chem. Solids* **1962**, *23*, 103.
[27] a) A. R. Miedema, *J. Less-Common Met.* **1973**, *32*, 117. b) A. R. Miedema, *J. Less-Common Met.* **1976**, *46*, 67. c) A. R. Miedema, R. Boom, F. R. DeBoer, *J. Less-Common Met.* **1975**, *41*, 283.
[28] a) J. St. John, A. N. Bloch, *Phys. Rev. Lett.* **1974**, *33*, 1095. b) A. Bloch, G. C. Schatteman, in *Structure and Bonding in Crystal* (Eds: A. Navrotsky, M. Okeeffe), Academic Press, New York **1981**.
[29] J. R Chelikowsky, J. C. Phillips, *Phys. Rev. B* **1978**, *17*, 2453.
[30] a) A. Zunger, *Phys. Rev. B* **1980**, *22*, 5839. b) A. Zunger, M. L. Cohen, *Phys. Rev. Lett.* **1978**, *41*, 53.
[31] D. G. Pettifor, *Solid State Commun.* **1984**, *51*, 31.
[32] P. Villars, K. Brandenburg, M. Berndt, S. LeClair, A. Jackson, Y.-H. Pao, B. Igelnik, M. Oxley, B. Bakshi, P. Chen, S. Iwata, *J. Alloys Compd.* **2001**, *317–318*, 26.
[33] If we included more compounds than Muller and Roy using their coordinates, we find about 30 more errors, e.g, $In_2BaO_4$ (spinel while assigned to be b9), $Cr_2BaO_4$ (spinel to b9), $Sb_2MgO_4$ (d1 to spinel), $Sb_2ZnO_4$ (d1 to spinel), $Pb_2SnO_4$ (d1 to b1), etc.
[34] a) R. D. Shannon, C. T. Prewitt, *Acta Cryst. B* **1969**, *25*, 925. b) R. D. Shannon, C. T. Prewitt, *Acta Cryst. B* **1970**, *26*, 1046.
[35] a) A. Zunger, S. Topiol, M. A. Ratner, *Chem. Phys.* **1979**, *39*, 75. b) A. Zunger, M. A. Ratner, *Chem. Phys.* **1978**, *30*, 423. c) S. Topiol, A. Zunger, M. A. Ratner, *Chem. Phys. Lett.* **1977**, *49*, 367.

[36] A. Zunger, M. L. Cohen, *Phys. Rev. B* **1978**, *18*, 5449.
[37] R. D. Shannon, *Acta Cryst. A* **1976**, *32*, 751.
[38] a) E. Fermi, E. Amaldi, *Accad. Ital. Rome* **1934**, *6*, 119. b) J. C. Phillips, L. Kleinman, *Phys. Rev.* **1959**, *116*, 287. c) A. Zunger, *J. Vac. Sci. Technol.* **1979**, *16*, 1337. d) P. A. Christiansen, K. S. Pitzer, *Chem. Phys. Lett.* **1982**, *85*, 434.
[39] A pseudopotential is undefined until a specific, physically motivated and deterministic choice is made. This is no different than the choice of tetrahedral versus octahedral ionic radii in inorganic chemistry, or the choice of a particular electronegativity scale: it is non-unique until one makes a motivated choice that renders it unique. The success or failure of the choice of a chemical scale is decided by testing its usefulness.
[40] As an illustration, the $\chi_{2s}(r)$ pseudo orbital of a first row element such as carbon was taken as $\chi_{2s}(r) = C_{1s,2s}\psi_{1s}(r) + C_{2s,2s}\psi_{2s}(r)$ with $C^2_{1s,2s} + C^2_{2s,2s} = 1$ and $C_{1s,2s}$ selected so as to shift the single-node of $\psi_{2s}(r)$ into the origin $r$=0.
[41] A. Zunger, in *Structure and Bonding in Crystals, Vol. I* (Ed.: M. Okeeffe, A. Navrotsky) Academic Press, New York **1981**, pp. 73135.
[42] C.-Y. Yeh, Z. W. Lu, S. Froyen, A. Zunger, *Phys. Rev. B* **1992**, *46*, 10086.
[43] a) P. Villars, *J. Less-Common Met.* **1983**, *92*, 215. b) P. Villars, *J. Less-Common Met.* **1986**, *119*, 175. c) P. Villars, J. C. Phillis, *Phys. Rev. B* **1988**, *37*, 2345.
[44] L. Pauling, *J. Am. Chem. Soc.* **1927**, *49*, 765.
[45] L. Pauling, *The Nature of The Chemical Bond*, Cornell University Press, New York **1960**.